

RESEARCH ARTICLE

MRpro – open PyTorch-based MR reconstruction and processing package

Felix Frederik Zimmermann¹ | Patrick Schuenke¹ | Christoph S. Aigner^{1,3} | Bill A. Bernhardt¹ | Mara Guastini¹ | Johannes Hammacher¹ | Noah Jaitner² | Andreas Kofler¹ | Leonid Lunin¹ | Stefan Martin¹ | Catarina Redshaw Kranich¹ | Jakob Schattenfroh² | David Schote¹ | Yanglei Wu² | Christoph Kolbitsch¹

¹Physikalisch-Technische Bundesanstalt (PTB), Braunschweig and Berlin, Germany

²Department of Radiology, Charité – Universitätsmedizin Berlin, Berlin, Germany

³Max Planck Research Group MR Physics, Max Planck Institute for Human Development, Berlin, Germany

Correspondence

Felix Frederik Zimmermann,
Physikalisch-Technische Bundesanstalt (PTB), Abbestrasse 2-12, 10587 Berlin, Germany Email: felix.zimmermann@ptb.de

Funding Information

This work was supported in part by the Metrology for Artificial Intelligence for Medicine (M4AIM) Project that is funded by the German Federal Ministry for Economic Affairs and Climate Action (BMWi) in the framework of the QI-Digital initiative and in part by the Deutsche Forschungsgemeinschaft (DFG, German Research Foundation) under Grant Nos. 289347353 (GRK2260, BIOQIC) and 372486779 (SFB1340) and in part by the European Partnership on Metrology, co-financed from the European Union's Horizon Europe Research and Innovation Programme and by the Participating States under Grant 22HLT02 A4IM.

Abstract

Purpose: To enable reproducible MR image reconstruction and quantitative parameter estimation.

Methods: We introduce MRpro, an open-source image reconstruction package built upon PyTorch and open data formats. The framework comprises three main areas. First, it provides unified data structures for the consistent manipulation of MR datasets and their associated metadata (e.g., k-space trajectories). Second, it offers a library of composable operators, proximable functionals, and optimization algorithms, including a unified Fourier operator for all common trajectories and an extended phase graph simulation for quantitative MR. These components are used to create ready-to-use implementations of key reconstruction algorithms. Third, for deep learning, MRpro includes essential building blocks such as data consistency layers, differentiable optimization layers, and state-of-the-art backbone networks and integrates public datasets to facilitate reproducibility. MRpro is developed as a collaborative project supported by automated quality control.

Results: We demonstrate the versatility of MRpro across multiple applications, including Cartesian, radial, and spiral acquisitions; motion-corrected reconstruction; cardiac MR fingerprinting; learned spatially adaptive regularization weights; model-based learned image reconstruction and quantitative parameter estimation.

Conclusion: MRpro offers an extensible framework for MR image reconstruction. With reproducibility and maintainability at its core, it facilitates collaborative development and provides a foundation for future MR imaging research.

KEYWORDS:

Image reconstruction, PyTorch, Deep Learning, Open-Source, Reproducible Research

Submitted to Magnetic Resonance in Medicine

1 | INTRODUCTION

In the last 25 years, MR image reconstruction has become more and more important in achieving the best possible image quality. A wide range of different approaches have been proposed that try to maximize the diagnostic output of the reconstructed images while minimizing the required raw k-space data, and hence reduce scan times^{1,2}. Currently, machine learning (ML) techniques are widely used in MR image reconstruction, pushing the boundaries of image reconstruction^{3,4,5,6,7}.

One major challenge of advanced image reconstruction techniques is their reproducibility and comparability. Even if the code is published open-access, it often requires dedicated MR sequences, which are not readily available, custom formats for raw k-space data, or the methods are only applicable to very specific use cases. In addition, long-term support and bug fixes are generally not guaranteed. All of this makes it very difficult to verify results, compare them with other methods, and build on the developments.

Two important milestones in standardizing MR image reconstruction were the specification of a vendor-independent, open-source format for raw MR data (ISM-RMRD)⁸ and the development of open-source reconstruction software. Prominent examples of the latter are Gadgetron⁹ and the Berkeley Advanced Reconstruction Toolbox (BART)¹⁰. Gadgetron is designed for rapid processing of incoming data streams, mainly targeting online reconstruction, whereas BART primarily targets offline reconstruction and methods development. Both frameworks include GPU-accelerated CUDA implementations of the Fast Fourier Transform (FFT) and Non-uniform FFT (NUFFT) to accelerate the reconstruction of data acquired with Cartesian and non-Cartesian trajectories. A primary challenge is that both frameworks are implemented in either C or C++. While this choice improves computational performance, it complicates integration with machine learning (ML) frameworks such as PyTorch¹¹ or JAX¹². BART addresses this by providing custom automatic differentiation functionality required for ML¹⁰. However, this approach increases the maintenance burden, as new ML building blocks must be reimplemented within the reconstruction framework. Consequently, although Gadgetron and BART provide MATLAB and Python interfaces, contributing to their core functionality requires extensive C or C++ knowledge. This presents a significant barrier for researchers accustomed to the Python-dominated environment of ML research and algorithm development.

This work introduces **MRpro**, a PyTorch-based, open-source framework for MR image reconstruction and

quantitative parameter estimation. The key features of **MRpro** include:

- implementation in PyTorch, ensuring seamless compatibility with ML methods.
- modular design facilitating development of complex reconstruction pipelines in Python.
- extensive library of predefined operators and algorithms.
- input/output using standardized ISMRMRD⁸ and DICOM format.
- dedicated data structures for unified handling of k-space data, sampling trajectories, and acquisition metadata.
- k-space trajectory calculation from Pulseseq¹³ files with automatic configuration of the corresponding Fourier operators.
- automatic quality control and continuous integration tests using phantom and in-vivo data.

2 | METHODS

The following provides an overview of the software design and highlights key aspects of **MRpro** (Figure 1). For more detailed information, we refer to the documentation at <https://docs.mrpro.rocks>. Several selected applications of **MRpro** are then described in detail to demonstrate the flexibility and power of **MRpro**.

The package **MRpro** is structured around three main thematic blocks: data handling, mathematical tools, and neural networks.

2.1 | Data handling

We focus on open data formats, choosing ISMRMRD as the preferred format for raw data import and export, and DICOM or NIFTI for image data. Trajectory information can also be imported from ISMRMRD files or directly from Pulseseq¹³ sequences. **MRpro** utilizes specialized container classes to store k-space data, quantitative parameter maps, and images. These containers hold both the data and its associated metadata, including acquisition information, orientation, position, and k-space trajectories. This design ensures coherent data manipulation; for example, selecting a subset of a **KData** object along the phase-encoding dimension also subsets the corresponding trajectory and acquisition metadata. All data containers can be moved to GPU memory for accelerated processing. Additionally, the framework provides human-readable descriptions and summary statistics to facilitate rapid data exploration and preprocessing.

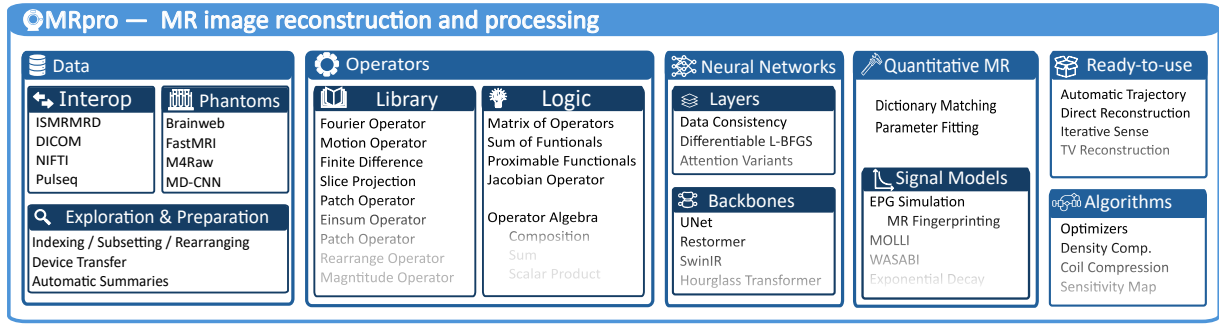


FIGURE 1 High-level overview of MRpro, covering data handling, a library of composable operators, DL layers and common backbone networks, algorithms, and signal models for qMRI. For more details, see the main text.

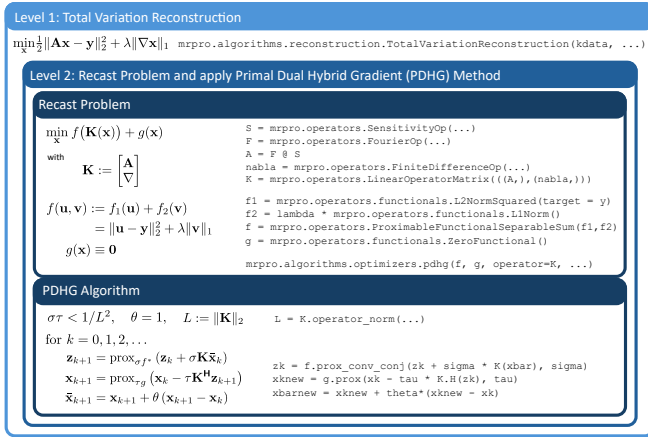


FIGURE 2 Software structure showing the different levels of abstractions for different components of a TV-minimization based image reconstruction. At the highest level (Level 1), the user calls the TV-reconstruction on a `KData` object. At a lower level (Level 2), the original problem is first recast to be able to use PDHG, where different mathematical objects (operators and functionals) are set up. Finally, PDHG computes the operator norm of the stacked operator \mathbf{K} and calls the proximal operators and convex conjugate of proximal operators of functionals in the algorithm.

2.2 | Mathematical Framework

A core component of MRpro is a framework of composable mathematical operators and functionals.

We provide a library of MR related operators, for example, a general Fourier acquisition operator (for Cartesian and non-Cartesian trajectories), a motion operator, and a volume-to-slice projection operator. These are implemented as instances of a `LinearOperator` class, and have associated Hermitian operators. For proper lower semi-continuous convex functionals, such as the squared ℓ_2 -norm or the ℓ_1 -norm,

MRpro implements their proximal operators and the proximal operators of their convex conjugates. All these components can be chained, stacked, and differentiated.

This modularity is leveraged to implement several important algorithms. These include the Conjugate Gradient (CG) method for solving linear systems $\mathbf{M}\mathbf{x} = \mathbf{b}$ with a symmetric, positive-definite \mathbf{M} , as required for iterative SENSE^{1,14} or within alternating minimization schemes¹⁵. The package also implements accelerated proximal gradient methods (FISTA/ISTA), for applications like wavelet-based compressed sensing^{16,17} and the Primal-Dual Hybrid Gradient (PDHG) algorithm, for example for reconstructions regularized by Total Variation (TV)^{18,19}.

Additionally, MRpro includes implementations of other common MR-specific algorithms, such as coil sensitivity estimation^{20,21}, density compensation, and coil compression²².

2.3 | Integration with DL

Basing MRpro on PyTorch provides native automatic differentiation and GPU acceleration for all operators and algorithms and enables seamless integration with the broader ML ecosystem. We provide implementations of state-of-the-art image-to-image network, such as U-Net²³, Attention U-Net²⁴, Restormer²⁵, Uformer²⁶, SwinIR²⁷, DC-AE²⁸, and Hourglass transformer²⁹. These architectures are adapted to accept additional conditioning inputs³⁰, allowing them to serve as backbones in MR reconstruction networks. In addition to the building blocks required for these networks, such as various attention mechanisms, MRpro includes multiple data consistency layers for physics-informed learning. These include a gradient-descent layer, an analytic data consistency layer for single-coil Cartesian data³¹, and a CG-based layer for multi-coil or non-Cartesian imaging³. For quantitative MR (qMRI), we implement a

differentiable L-BFGS solver³² based on implicit differentiation^{33,34} to enforce consistency with the signal model. Furthermore, we integrate several well-known publicly available datasets for training and evaluation, including fastMRI³⁵, BrainWeb³⁶, M4Raw³⁷ and the MD-CNN dataset³⁸ which can be used for both training and evaluation.

2.4 | Automatic reconstruction

The main building block of any MR image reconstruction is the Fourier transform. The type of Fourier transform depends on the k-space trajectory, e.g., FFT for Cartesian acquisitions and NUFFT for non-Cartesian acquisitions such as radial or spiral. For a proper reconstruction detailed knowledge about the actual implementation of the k-space trajectory is required and needs to be provided to the reconstruction algorithm.

In **MRpro**, all information describing advanced Cartesian acquisition schemes (undersampling, partial Fourier, reversed readouts, etc) are imported from ISMRMRD. For non-Cartesian acquisition schemes, some commonly used trajectories such as radial sampling are implemented. But, rather than having to implement custom sampling schemes in **MRpro**, trajectory information can also be provided as part of the ISMRMRD raw data file. Finally, **MRpro** also allows for the automatic calculation of the trajectory from a provided Pulseseq sequence file. Based on the trajectory information stored in the **KData** instance, a Fourier operator can be instantiated. The required Fourier operations are automatically selected, i.e., the dimensions along which FFT or NUFFT operations have to be applied, are identified without any user input. Furthermore, a matching density compensation function is calculated. This means that data obtained with arbitrary trajectories can be reconstructed from a MR raw data file and the corresponding Pulseseq sequence file without any additional inputs. This is especially of interest for researchers who want to focus on the optimisation of reconstruction algorithms and are less experienced with MR data acquisition. Further, we provide ready-to-use high-level implementations of well-known reconstruction algorithms (e.g., Iterative SENSE or TV-regularized reconstructions). These include all necessary steps to obtain images based on the imported **KData** alone. This, on the other hand, allows researchers who focus on sequence development to perform reproducible reconstructions without requiring a deep understanding of reconstruction algorithms.

2.5 | Quantitative parameter estimation

MRpro provides several differentiable MR signal models ranging from simple mono-exponential T_1 or T_2 , Modified Look-Locker Inversion recovery (MOLLI)³⁹, Watershift and B1 mapping (WASABI)⁴⁰ to an extended phase graph⁴¹ (EPG) simulation (for example, for cardiac MR fingerprinting^{42,43}). The models calculate signals from multi-dimensional parameter inputs and are defined as (non-linear) **Operator**, which can be easily combined with other operators. In order to fit a T_1 inversion-recovery model to magnitude images, for example, the signal model operator can be combined with the magnitude operator to form a new model. Besides non-linear optimizers^{44,32} for parameter regression, **MRpro** also includes a dictionary matching operator (see [Section 2.7.4](#)).

2.6 | Community-based development, quality control and release

Built in Python and licensed under the Apache 2.0 license, **MRpro** is developed openly on GitHub to foster community collaboration and reproducibility.

High code quality, consistent coding practices, and adherence to established standards is enforced through a continuous integration (CI) pipeline, illustrated in [Figure 3](#). This pipeline automates static analysis (Ruff*, Mypy†) and a multi-level testing strategy. Unit tests maintain over 90% code coverage to verify individual components. The tests are in part run on GitHub servers, in part run on GPU accelerated nodes in our in-house compute cluster. Integration tests validate end-to-end functionality on realistic MRI reconstruction tasks and are subsequently converted into Jupyter notebooks, serving as executable examples within the documentation. Before a proposed code change is merged into the code base, all tests have to pass and the changes to the documentation and as well as the code are reviewed. We provide regular releases on both Github and PyPI. For backward compatibility, we follow the *Scientific Python*‡ recommendations, supporting the last three years of Python versions. Additionally, we provide full Docker images for reproducibility as well as docker recipes for use with Siemens OpenRecon system for online reconstruction§.

*<https://github.com/astral-sh/ruff>

†<https://github.com/python/mypy>

‡<https://scientific-python.org/>

§https://github.com/PTB-MR/mrpro_server

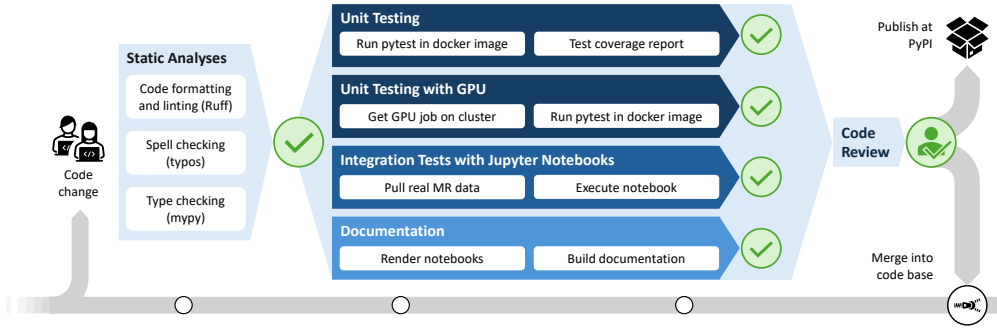


FIGURE 3 Flow chart of CI workflow for a pull request. Static checks, unit test and integration tests are executed. The integration tests are notebooks and also serve as examples in the documentation. After a manual code review, the change is merged.

2.7 | Experiments

In the following, we give an overview of image reconstruction and parameter estimation examples. If not stated otherwise, we consider variational reconstruction methods of the form

$$\min_{\mathbf{x}} \frac{1}{2} \|\mathbf{Ax} - \mathbf{y}\|_2^2 + \mathcal{R}(\mathbf{x}), \quad (1)$$

where \mathbf{A} denotes the linear forward operator (usually the composition of a Fourier operator, a coil-sensitivity operator, and possibly a motion operator), \mathbf{x} denotes the sought complex-valued MR image, \mathbf{y} the corresponding (often undersampled and noise-corrupted) k-space data, and \mathcal{R} an optional regularization functional for the image. Further, we also consider variational quantitative parametric estimation problems of the form

$$\min_{\mathbf{p}} \frac{1}{2} \|\mathbf{Aq}(\mathbf{p}) - \mathbf{y}\|_2^2 + \mathcal{S}(\mathbf{p}), \quad (2)$$

with \mathbf{q} denoting a non-linear voxel-wise signal model (e.g., inversion recovery, saturation recovery) and \mathbf{p} the quantitative parametric maps of interest (e.g., M_0 , T_1 , T_2), and \mathcal{S} a regularization functional for the parametric maps. Each of the following examples also contains a Jupyter notebook as part of the **MRpro** repository[¶]. These notebooks contain more information about the reconstruction problem and give a more detailed step-by-step guide of how to solve it. They are run automatically as part of the continuous integration tests and the output, i.e., reconstructed images and parameter maps, can be viewed in the documentation[#].

All data shown here was obtained with either a 3 T SiemensCima.X, a 3 T Siemens Lumina scanner, or a 55 mT OSI² ONE, and is made publicly available, or is part of well-known public datasets³⁵. All in-vivo scans were approved by the local ethics committees and were carried out in accordance with relevant guidelines and regulations. The subjects gave written informed consent to participate in this study.

2.7.1 | Cartesian image reconstruction

Most MR scans use a Cartesian sampling scheme to acquire the k-space data. In **MRpro**, Cartesian trajectories are calculated directly from the data acquisition indices in the ISMRMRD header. A Cartesian sampling operator maps between a rectilinear fully-sampled k-space and the points sampled in the acquisition. This operator is designed to handle various acquisition schemes, including partial echo, partial Fourier, and undersampling with random k-space masks. The Cartesian sampling operator is automatically created based on the trajectory as part of the Fourier operator.

As an example, we acquired a T_1 -weighted 2D Cartesian brain scan using a vendor's self-calibrated SENSE sequence. Coil sensitivity maps were estimated from the auto-calibration lines in the k-space center. Image reconstruction in **MRpro** was performed by solving the problem in Equation 1 without regularization, i.e., with $\mathcal{R}(\mathbf{x}) \equiv 0$, using the ready-to-use CG-SENSE implementation. We performed this reconstruction via two pathways: offline, after exporting the raw data to the ISMRMRD format, and online, using the Siemens OpenRecon framework. For the online reconstruction, the acquired raw data stream was sent directly to a container running **MRpro**, which reconstructed the images and forwarded them to the console for viewing. The raw data and the vendor's DICOM reconstruction are available on Zenodo⁴⁵.

2.7.2 | Motion-corrected image reconstruction

Physiological motion, such as respiration, can severely degrade MR image quality, particularly in high-resolution 3D acquisitions⁴⁶. While respiratory gating mitigates these artifacts, it increases scan time. Motion-corrected reconstruction techniques have been proposed to address this by computationally compensating for motion, enabling high-quality imaging from data acquired in different motion states⁴⁷.

[¶]<https://github.com/PTB-MR/mrpro/blob/main/examples/notebooks>

[#]<https://docs.mrpro.rocks/examples.html>

We demonstrate such a motion-corrected reconstruction in **MRpro** using a free-breathing, 3D Golden-Angle Radial Phase Encoding (RPE) acquisition of the thorax and abdomen^{48,49}. The data and the Pulseseq file used for the acquisition are available on Zenodo⁵⁰. The reconstruction process involves several steps. First, a self-navigator signal is extracted from the central k-space profile of each readout and used to bin the data into discrete respiratory motion states. A set of motion-resolved images is then reconstructed using an iterative algorithm with TV-regularization across both spatial and motion dimensions⁵¹. Next, non-rigid motion fields between each motion state and a reference state are estimated from these images using the Medical Image Registration Toolkit (MIRTK)⁵². These displacement fields are used to construct a motion operator that describes the transformation from a reference motion state to the other motion states and is incorporated into the forward model **A**. Finally, a single, high-quality motion-corrected image is obtained by solving an unregularized least-squares problem, i.e., Equation 1 with $\mathcal{R}(\mathbf{x}) \equiv 0$.

2.7.3 | Learning spatially adaptive regularization parameter maps for TV-based reconstruction

In TV-based reconstruction, using a single regularization parameter that globally dictates the strength of the TV regularization, i.e., $\mathcal{R}(\mathbf{x}) = \lambda \|\nabla \mathbf{x}\|_1$ with $\lambda > 0$ in Equation 1, is suboptimal. Instead, locally adapting the regularization strength by employing parameter maps can substantially improve the resulting reconstructions⁵³. A recent DL method for estimating regularization parameter maps for TV-based reconstruction⁵⁴ consists of two main blocks. First, a convolutional neural network (CNN), \mathcal{N}_Θ , is applied to an initial estimate of the image \mathbf{x}_0 to estimate suitable regularization parameter maps, i.e., $\Lambda_\Theta := \mathcal{N}_\Theta(\mathbf{x}_0)$. Second, an unrolled PDHG scheme of finite length solves the problem

$$\min_{\mathbf{x}} \frac{1}{2} \|\mathbf{A}\mathbf{x} - \mathbf{y}\|_2^2 + \|\Lambda_\Theta \nabla \mathbf{x}\|_1 \quad (3)$$

assuming the regularization parameter maps are fixed. The entire reconstruction network can be trained end-to-end; thus, \mathcal{N}_Θ learns to estimate regularization parameter maps such that the resulting reconstructions are as close as possible to the target images. This method can be easily implemented in **MRpro** by providing $\mathcal{N}_\Theta(\mathbf{x}_0)$ as a **weight** parameter to the functional f_2 in Figure 2 to define a weighted ℓ_1 -norm.

We trained the network on simulated data based on the BrainWeb dataset³⁶. We then applied the trained network to a fully-sampled, in-vivo brain scan acquired

on an OSI² ONE open-source^{||} ultra-low-field scanner^{55,56,57}.

2.7.4 | Cardiac magnetic resonance fingerprinting

Cardiac magnetic resonance fingerprinting (cMRF) is a highly efficient approach to estimate T_1 - and T_2 -maps of the heart in a single scan^{58,42}.

We showcase the reconstruction of a cMRF sequence and the subsequent estimation of T_1 - and T_2 -maps from data acquired on the T1MES phantom⁵⁹. An open-source spiral cMRF sequence⁴³ with T_1 -inversion pulses and T_2 -preparation pulses was used triggered by a simulated ECG signal. The data can be found on Zenodo⁶⁰.

The reconstruction begins by obtaining qualitative dynamic images using a sliding window approach. Next, a signal dictionary is created using the Extended Phase Graph (EPG)⁴¹ method simulating signal evolutions for T_1 values between 50 ms and 2 s and T_2 values between 6 ms and 200 ms. Finally, the parameter maps are estimated by matching the measured signal evolution of each pixel to the dictionary entries. Specifically, for a given pixel's measured signal evolution \mathbf{x} , the index k^* of the best-matching dictionary entry \mathbf{d}_k is found by maximizing the normalized dot product⁵⁸,

$$k^* = \arg \max_{k \in \{1, \dots, K\}} \left| \left\langle \frac{\mathbf{d}_k}{\|\mathbf{d}_k\|_2}, \frac{\mathbf{x}}{\|\mathbf{x}\|_2} \right\rangle \right|. \quad (4)$$

The quantitative parameters $\mathbf{p}_{k^*} = (T_1, T_2)_{k^*}$ associated with this index are then assigned to the pixel. This operation is repeated across all pixels to form the final parameter maps. Sliding-window image reconstruction, EPG simulation, and dictionary matching are all implemented in **MRpro**.

As reference methods, we used multi-echo spin-echo (T_2) and multi-inversion-time spin-echo (T_1) sequences.

2.7.5 | Model-based DL

In *MoDL*³, the regularization in Equation 1 is learned, i.e. $\mathcal{R} = \mathcal{R}_\Theta$ where Θ denote parameters of a CNN \mathcal{N}_Θ . The problem is solved by alternating between the CNN for denoising/artifact removal and a data consistency update. Specifically, starting with an initial reconstruction \mathbf{x}_0 , the updates for $k = 1, \dots, T$, are given

^{||} <https://www.opensourceimaging.org/project/osii-one/>

by

$$\mathbf{z}_k := \mathcal{N}_\Theta(\mathbf{x}_k) \quad (5)$$

$$\mathbf{x}_{k+1} := \arg \min_{\mathbf{x}} \frac{1}{2} \|\mathbf{A}\mathbf{x} - \mathbf{y}\|_2^2 + \frac{\lambda}{2} \|\mathbf{x} - \mathbf{z}_k\|_2^2, \quad (6)$$

where the learned parameter $\lambda > 0$ balances the data consistency and the CNN.

With **MRpro**, the construction of necessary operators, the integration of neural networks as well as an efficient differentiable solution mapping for solving Equation 6 are available, making it easy to implement MoDL with only a few lines of code. We implemented MoDL matching the original formulation in the number of iterations (10), the CNN architecture and the use of weight sharing. We used a CG operator with an explicit implementation of the derivative, thereby avoiding storing intermediate results for back-propagation^{3,34}. We applied MoDL to Cartesian 8-fold 2D random accelerated fastMRI³⁵ T_1 -weighted axial brain data with sensitivity maps estimated once from k-space center²⁰. The model was trained for a single epoch without augmentations, optimizing a loss function that equally weighted mean squared error and structural similarity index⁶¹ (SSIM).

2.7.6 | End-to-end training of physics informed quantitative imaging

A recent DL approach, *PINQI*³⁴, approaches the solution of Equation 2 by half quadratic splitting to alternate between two subproblems. The first is a linear image reconstruction task

$$\min_{\mathbf{x}} \frac{1}{2} \|\mathbf{A}\mathbf{x} - \mathbf{y}\|_2^2 + \frac{\lambda_{\mathbf{x}}}{2} \|\mathbf{x} - \mathbf{x}_{\text{reg}}\|_2^2 + \frac{\lambda_{\mathbf{q}}}{2} \|\mathbf{q}(\mathbf{p}) - \mathbf{x}\|_2^2 \quad (7)$$

with \mathbf{x} being intermediary qualitative images, $\lambda_{\mathbf{x}}$ and $\lambda_{\mathbf{q}}$ being regularization strengths and \mathbf{x}_{reg} denoting an image prior for regularization. The second, non-linear, subproblem is finding the quantitative parameters by solving

$$\min_{\mathbf{p}} \frac{\lambda_{\mathbf{q}}}{2} \|\mathbf{q}(\mathbf{p}) - \mathbf{x}\|_2^2 + \frac{\lambda_{\mathbf{p}}}{2} \|\mathbf{p} - \mathbf{p}_{\text{reg}}\|_2^2. \quad (8)$$

Here, \mathbf{p}_{reg} is a prior on the parameter maps and $\lambda_{\mathbf{p}}$ the associated weight for regularization. In *PINQI*, a solution to Equation 2 is found by iterating between both subproblems. In each iteration $k = 1, \dots, T$, the image and parameter priors are updated by U-Nets as $\mathbf{x}_{\text{reg},k} = \mathcal{N}_\Theta(\mathbf{x}_{k-1})$ and $\mathbf{p}_{\text{reg},k} = \mathcal{P}_\Phi(\mathbf{x}_k)$, respectively. The network parameters Θ and Φ , and the regularization strengths are trained end-to-end. This requires that the subproblems are solved using differentiable optimization to allow gradient flow to the network parameters. **MRpro** provides flexible operators for differentiable optimization as well as network backbones to implement *PINQI*.

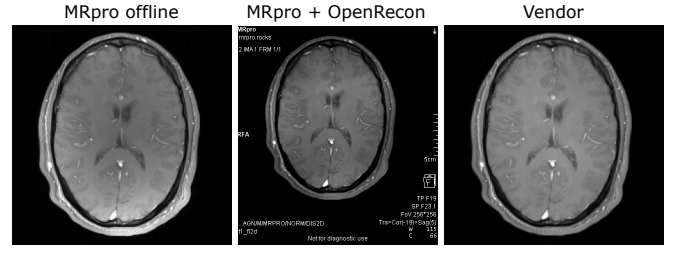


FIGURE 4 Comparison of a 2-fold accelerated Cartesian SENSE reconstruction performed offline with **MRpro**, online using the Siemens OpenRecon framework with **MRpro**, and the standard clinical vendor pipeline. Intensity variations between the reconstructions are due to difference in the coil map estimation.

We evaluated this implementation on a T_1 -mapping task simulating a saturation recovery experiment using the BrainWeb dataset. The signal model for the parameter maps $\mathbf{p} = [\mathbf{M}_0, \mathbf{T}_1]^T$ stacks the signals from $S = 5$ different saturation times t_i , where each component is given by $q_i(\mathbf{M}_0, \mathbf{T}_1) = \mathbf{M}_0(1 - e^{-t_i/\mathbf{T}_1})$. We simulated an 8-fold random Cartesian undersampling of the k-space data of the qualitative images (matrix size 192×192). For comparison, we performed a classical two-step reconstruction using CG-SENSE followed by a pixel-wise non-linear least-squares regression of the signal model.

3 | RESULTS

3.1 | Direct image reconstruction

Figure 4 shows the results of a Cartesian image reconstruction. The **MRpro** reconstruction achieves image quality comparable to the vendor's. The residual intensity variations in the **MRpro** result are due to the multi-coil acquisition; the vendor reconstruction compensates for this using an additional body coil scan, a feature not yet available in **MRpro**.

3.2 | Motion-corrected image reconstruction

Figure 5 demonstrates the effectiveness of motion correction in **MRpro**. By using only self-navigator information already present in the acquired raw data, motion artifacts can be substantially reduced and image quality improved.

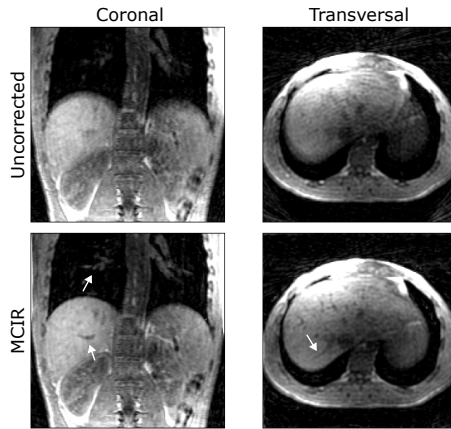


FIGURE 5 Motion-corrected image reconstruction. The uncorrected image shows blurring from respiratory motion. Incorporating motion information into the model (MCIR) yields a corrected image with improved depiction of the liver, kidneys, and vessels (white arrows).

3.3 | Learning spatially adaptive regularization for TV-based reconstruction

Figure 6 shows the results for a learned spatially adaptive TV-based reconstruction. In the simulated experiment using BrainWeb data, the adjoint reconstruction is poor (SSIM=0.46). While TV reconstruction with an optimal scalar parameter improves the result (SSIM=0.72), the learned spatially adaptive parameter maps yield the best reconstruction (SSIM=0.78). Notably, the learned approach is superior even though the scalar baseline was optimized using an oracle line-search with access to the ground truth. Furthermore, the network trained on purely simulated data can also be transferred to in-vivo data acquired on an ultra-low-field scanner (Figure 6 b). This example showcases the implementation of the method⁵⁴ using MRpro's building blocks and confirms that DL can significantly enhance TV regularization.

3.4 | Cardiac magnetic resonance fingerprinting

Figure 7 shows the quantitative parameter maps of the T1MES phantom obtained using the cardiac MR fingerprinting sequence. A linear regression of the mean T_1 - and T_2 -values in each of the nine tubes shows good agreement between the result obtained by MR fingerprinting and the spin-echo reference methods ($R^2 > 0.99$).

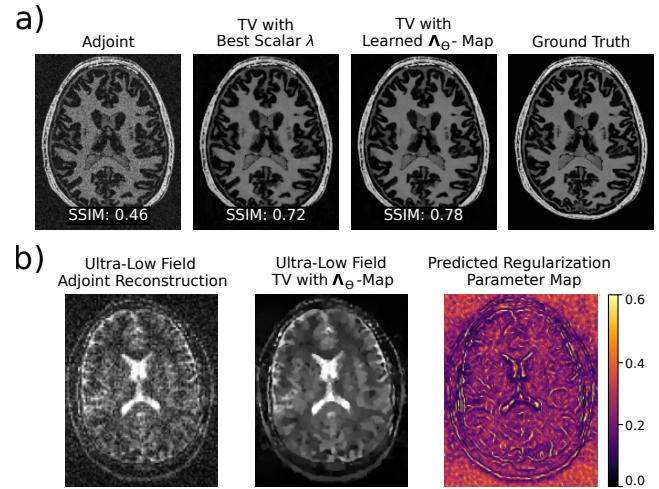


FIGURE 6 Learning spatially adaptive regularization parameter maps for TV-reconstruction. a) Results for a *simulated* ultra-low-field MRI based on the BrainWeb³⁶ dataset. From left to right: adjoint reconstruction, TV-reconstruction with the best scalar lambda (obtained by line search using the ground truth image), TV-reconstruction with estimated spatially adaptive regularization parameter maps, and the ground truth image. b) Application of the network trained on simulated data to *in-vivo* data obtained from an OSI² ONE ultra-low-field scanner. From left to right: adjoint reconstruction, TV-reconstruction with the regularization parameter map predicted by the network, predicted regularization parameter map.

3.5 | Model-based DL

Figure 8 shows a comparison of various reconstruction methods applied to an 8-fold accelerated brain scan from the multi-coil fastMRI dataset³⁵ with random 2D Cartesian undersampling. As baselines, we compare with a zero-filled adjoint reconstruction and CG-SENSE, all implemented in MRpro. MoDL achieves the highest SSIM of 0.95, reproducing the results of Aggarwar et al.³

3.6 | End-to-end training of physics informed quantitative imaging

The results of T_1 -mapping from a undersampled saturation recovery sequence using PINQI are shown in Figure 9. While the classical reconstruction fails to remove undersampling artefacts (T_1 SSIM 0.42, nRMSE 0.11), our implementation of PINQI in MRpro reproduces the reported performance³⁴ with an SSIM of 0.93 and an nRMSE of 0.03.

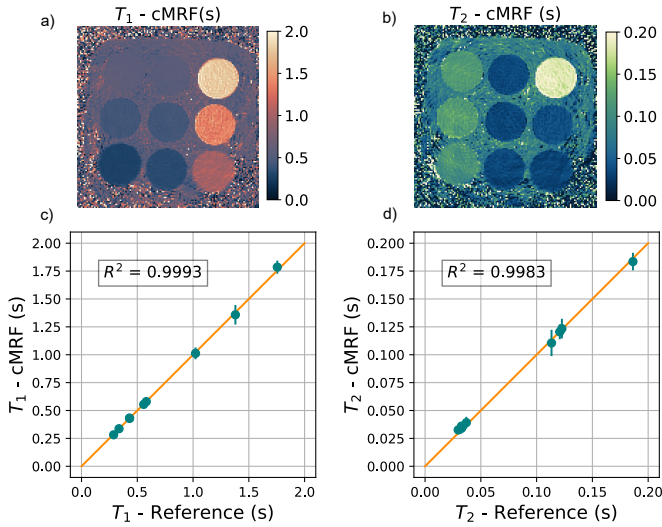


FIGURE 7 T_1 -map (a) and T_2 -map (b) of the TIMES phantom from an open-source spiral cMRF sequence. The comparison of mean T_1 (c) and T_2 (d) values within each tube of the phantom to reference values from spin-echo sequences demonstrates high agreement over the full range of values.

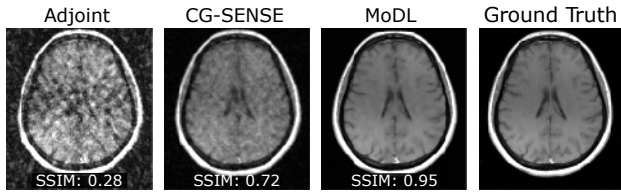


FIGURE 8 Comparison of reconstructed images from accelerated fastMRI³⁵ brain data using different methods. From left to right: adjoint reconstruction (SSIM = 0.28), CG-SENSE¹⁴ (SSIM = 0.72), and MoDL³ (SSIM = 0.95), ground truth image.

4 | DISCUSSION

In this work, we introduced **MRpro**, a modular, open-source framework designed to bridge the gap between advanced MRI reconstruction and the rapidly evolving field of Python-based machine learning. The discussion below contextualizes **MRpro** within the existing software landscape, highlights its demonstrated capabilities, and outlines its limitations and future directions.

Several software packages address aspects of MR reconstruction. The core value proposition of **MRpro** is its unified, PyTorch-native environment, offering MR specific data structures and an extensive library of operators and mathematical tools for combining classical reconstruction algorithms with state-of-the-art DL approaches. While high-performance C/C++ frameworks like BART¹⁰ and Gadgetron⁹ offer computational speed

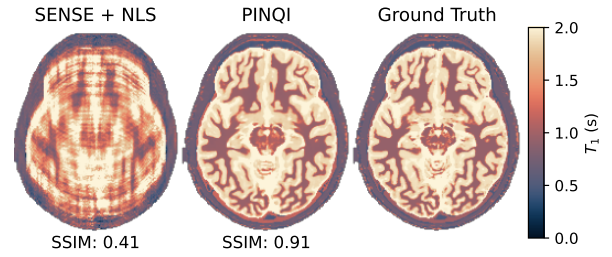


FIGURE 9 Results for an implementation of *PINQI*³⁴: On a synthetic BrainWeb³⁶ based saturation recovery T_1 -mapping dataset at 8x Cartesian undersampling, the physics informed approach to learned quantitative imaging (center) outperforms the classic reconstruction (left), i.e., SENSE followed by non-linear least squares (NLS).

but present a significant barrier, especially for ML researchers accustomed to Python. Conversely, general-purpose Python libraries for inverse problems, such as ODL⁶² and DeepInverse⁶³, provide composable operators but lack the specialized, out-of-the-box support for MRI-specific data structures, operators (e.g., non-Cartesian trajectories, partial Fourier), and processing workflows. Other Python toolboxes are more closely related but have distinct goals. SigPy⁶⁴ provides excellent signal processing blocks but is not natively built on PyTorch, creating friction for deep learning integration. DIRECT⁶⁵ focuses on comparisons of DL methods and application to Cartesian reconstruction challenges, less on providing building blocks for general MR reconstruction tasks. MONAI⁶⁶ mainly focuses on image generation⁶⁷ and image segmentation, offering many implementations of common networks for these tasks. TorchIO⁶⁸ provides datasets of medical images and image augmentations. Complex-valued data and raw k-space data with accompanying metadata are not supported. Finally, only few solutions exist for qMRI, such as PyQMRI⁶⁹ and qMRLab⁷⁰, neither of which integrates with DL frameworks. Thus, while there exist many related software solutions, **MRpro** is specifically designed to fill these gaps, offering a unified, PyTorch-native environment for both classical and ML reconstruction research.

The framework's commitment to open standards like ISMRMRD, DICOM, and the vendor agnostic sequence standard Pulseseq promotes reproducibility⁷¹ and enables seamless integration with both research systems, such as the OSI² low-field MRI using the Nexus console⁵⁷ (Section 2.7.3), and clinical scanners (Figure 4). For Siemens systems, our OpenRecon container allows the usage of **MRpro** directly at the scanner (Figure 4). **MRpro** is designed in a modular way starting with basic building blocks such as data objects, operators including

signal models and solvers. These are combined to ready-to-use reconstruction pipelines (e.g. TV-regularised iterative image reconstruction or iterative SENSE). We have shown how custom algorithms can be created using the provided building blocks. We demonstrated this for motion corrected reconstruction (Section 2.7.2) and three diverse DL approaches: MoDL³ (Section 3.5), learned regularization maps⁵⁴ (Section 2.7.3), and PINQI³⁴ (Section 3.6). The framework's utility for quantitative MRI was not only validated through a cardiac fingerprinting application (Section 3.4), but also previously by securing a second-place award in the MRI Study Group challenge at ISMRM 2024 on T₁ and T₂* mapping. In the challenge, the data consisted of turbo-spin echo images obtained from a phantom at different time points after an inversion pulse⁷² and gradient echo images with different echo times for T₂* mapping⁷³. Our MRpro entry used dictionary matching to obtain a first estimate of the relaxation times, followed by a non-linear regression of the signal models using ADAM⁴⁴. Additionally, MRpro has been successfully used for the reconstruction of virtual phantom data simulated using MRzero^{74,71}, resulting in a fully differentiable MR simulator and reconstruction. This powerful combination paves the way for future advancements such as end-to-end MR pulse sequence optimization. Despite its flexibility, MRpro has limitations. Its foundation on PyTorch, while enabling GPU acceleration, automatic differentiation, seamless DL integration and rapid development, means it is not directly compatible with other frameworks like TensorFlow⁷⁵ or JAX¹². Focusing on a single backend framework increases maintainability and development velocity and allows for specific optimizations for that backend. We believe this trade-off is justified by PyTorch's prevalence in the MR reconstruction community.

While MRpro provides a robust foundation, including essential components for pre-whitening, coil compression, and sensitivity estimation, it does not yet include all established methods, such as ESPIRiT⁷⁶ or GRAPPA². The modular architecture and comprehensive continuous integration pipeline are explicitly designed to facilitate community contributions. We therefore invite the research community to extend MRpro by integrating these and other advanced methods, further enhancing its value as a shared tool for open and reproducible science.

5 | CONCLUSIONS

We presented an open-source image reconstruction packages which utilises PyTorch to allow for fast processing and native integration into DL approaches. MRpro follows a highly modular structure with low-level operators and

high-level image reconstruction algorithms. We demonstrated the capabilities of MRpro on a range of different reconstruction problems including motion-corrected image reconstruction, model-based DL and end-to-end quantitative imaging. All examples can be reproduced by freely available Jupyter notebooks and open-access data on Zenodo. The comprehensive quality control and testing framework of MRpro follows modern software development standards and will ensure longevity of this package.

Data Availability Statement

All the code to reproduce the results in this manuscript is available as Jupyter notebooks as part of the examples in MRpro^{**}. Each notebook can be run in Google Colab directly from the browser. The necessary data is freely available via Zenodo. Please see the notebooks for more details. Note: At time of submission some notebooks/features are not part of the main branch yet. They will be added to the main branch for the final publication.

Acknowledgment

We would like to thank Tom O'Reilly and Andrew Webb for providing the in-vivo data acquired on the OSI² ONE open-source low-field scanner.

Financial disclosure

The authors do not have any financial disclosures.

Conflict of interest

The authors declare no potential conflict of interests.

ORCID

Felix Frederik Zimmermann  0000-0002-0862-8973

Patrick Schuenke  0000-0002-3179-4830

Christoph S. Aigner  0000-0003-3618-9610

Bill A. Bernhardt  0009-0008-1973-9266

Mara Guastini  0009-0003-5460-0941


Johannes Hammacher  0009-0008-2764-6537

Noah Jaitner  0009-0002-5647-593X

Andreas Kofler  0000-0001-9169-2572

Leonid Lunin  0000-0001-6469-5532

Stefan Martin  0009-0009-0741-8534

Catarina Redshaw Kranich  0009-0008-3305-0342

^{**}<https://docs.mrpro.rocks/examples.html>

Jakob Schattenfroh  0009-0007-3654-4578

David Schote  0000-0003-3468-0676

Yanglei Wu  0000-0003-4819-9875

Christoph Kolbitsch  0000-0002-4355-8368

REFERENCES

1. Pruessmann Klaas P., Weiger Markus, Scheidegger Markus B., Boesiger Peter. SENSE: sensitivity encoding for fast MRI. *Magnetic Resonance Imaging*. 1999;42:952–962.
2. Griswold Mark A., Jakob Peter M., Heidemann Robin M., et al. Generalized autocalibrating partially parallel acquisitions (GRAPPA). *Magnetic Resonance in Medicine*. 2002;47:1202–1210.
3. Aggarwal Hemant K., Mani Merry P., Jacob Mathews. MoDL: Model-based deep learning architecture for inverse problems. *IEEE Transactions on Medical Imaging*. 2018;38(2):394–405.
4. Ravishankar Saiprasad, Ye Jong Chul, Fessler Jeffrey A.. Image Reconstruction: From Sparsity to Data-Adaptive Methods and Machine Learning. *Proceedings of the IEEE*. 2020;108:86–109.
5. Sriram Anuroop, Zbontar Jure, Murrell Tullie, et al. End-to-end variational networks for accelerated MRI reconstruction. In: *International conference on medical image computing and computer-assisted intervention* 2020:64–73.
6. Jalal Ajil, Arvinte Marius, Daras Giannis, Price Eric, Dimakis Alexandros G., Tamir Jon. Robust compressed sensing mri with deep generative priors. *Advances in neural information processing systems*. 2021;34:14938–14954.
7. Chen Yutong, Schonlieb Carola Bibiane, Lio Pietro, et al. AI-Based Reconstruction for Fast MRI-A Systematic Review and Meta-Analysis. *Proceedings of the IEEE*. 2022;110:224–245.
8. Inati Souheil J., Naegele Joseph D., Zwart Nicholas R., et al. ISMRM Raw data format: A proposed standard for MRI raw datasets. *Magnetic Resonance in Medicine*. 2017;77:411–421.
9. Hansen Michael Schacht, Sørensen Thomas Sangild. Gadgetron: an open source framework for medical image reconstruction. *Magnetic Resonance in Medicine*. 2013;69(6):1768–1776.
10. Blumenthal Moritz, Luo Guanxiong, Schilling Martin, Holme H. Christian M., Uecker Martin. Deep, deep learning with BART. *Magnetic Resonance in Medicine*. 2023;89(2):678–693.
11. Paszke Adam, Gross Sam, Massa Francisco, et al. PyTorch: an imperative style, high-performance deep learning library. Red Hook, NY, USA: Curran Associates Inc. 2019.
12. Frostig Roy, Johnson Matthew James, Leary Chris. Compiling machine learning programs via high-level tracing. *Systems for Machine Learning*. 2018;4(9).
13. Layton Kelvin J., Kroboth Stefan, Jia Feng, et al. Pulseq: A Rapid and Hardware-Independent Pulse Sequence Prototyping Framework. *Magnetic Resonance in Medicine*. 2017;77(4):1544–1552.
14. Pruessmann Klaas P., Weiger Markus, Börnert Peter, Boesiger Peter. Advances in sensitivity encoding with arbitrary k-space trajectories. *Magnetic Resonance in Medicine*. 2001;46(4):638–651.
15. Ramani Sathish, Fessler Jeffrey A.. Parallel MR Image Reconstruction Using Augmented Lagrangian Methods. *IEEE Transactions on Medical Imaging*. 2011;30(3):694–706.
16. Daubechies Ingrid, Defrise Michel, De Mol Christine. An iterative thresholding algorithm for linear inverse problems with a sparsity constraint. *Communications on Pure and Applied Mathematics: A Journal Issued by the Courant Institute of Mathematical Sciences*. 2004;57(11):1413–1457.
17. Lustig Michael, Donoho David, Pauly John M.. Sparse MRI: The application of compressed sensing for rapid MR imaging. *Magnetic Resonance Imaging*. 2007;58:1182–1195.
18. Chambolle Antonin, Pock Thomas. A first-order primal-dual algorithm for convex problems with applications to imaging. *Journal of mathematical imaging and vision*. 2011;40:120–145.
19. Knoll Florian, Unger Markus, Diwoy Clemens, Clason Christian, Pock Thomas, Stollberger Rudolf. Fast reduction of undersampling artifacts in radial MR angiography with 3D total variation on graphics hardware. *Magnetic Resonance Materials in Physics, Biology and Medicine*. 2010;23:103–114.
20. Inati Souheil J., Hansen Michael S., Kellman Peter. A Fast Optimal Method for Coil Sensitivity Estimation and Adaptive Coil Combination for Complex Images. In: *Proceedings of the 22nd Annual Meeting of ISMRM* 2014.
21. Walsh David O., Gmitro Arthur F., Marcellin Michael W.. Adaptive reconstruction of phased array MR imagery. *Magnetic Resonance in Medicine*. 2000;43(5):682–690.
22. Huang Feng, Vijayakumar Sathya, Li Yu, Hertel Sarah, Duensing George R.. A software channel compression technique for faster reconstruction with many channels. *Magnetic resonance imaging*. 2008;26(1):133–141.
23. Ronneberger Olaf, Fischer Philipp, Brox Thomas. U-net: Convolutional networks for biomedical image segmentation. *Medical image computing and computer-assisted intervention (MICCAI)*. 2015;part III 18:234–241.
24. Oktay Ozan, Schlemper Jo, Le Folgoc Loic, et al. Attention U-Net: Learning Where to Look for the Pancreas. In: *Medical Imaging with Deep Learning*.
25. Zamir Syed Waqas, Arora Aditya, Khan Salman, Hayat Munawar, Khan Fahad Shahbaz, Yang Ming-Hsuan. Restormer: Efficient transformer for high-resolution image restoration. In: *Proceedings of the IEEE/CVF conference on computer vision and pattern recognition* 2022:5728–5739.
26. Wang Zhendong, Cun Xiaodong, Bao Jianmin, Zhou Wengang, Liu Jianzhuang, Li Houqiang. Uformer: A general u-shaped transformer for image restoration. In: *Proceedings of the IEEE/CVF conference on computer vision and pattern recognition* 2022:17683–17693.

27. Liang Jingyun, Cao Jiezhong, Sun Guolei, Zhang Kai, Van Gool Luc, Timofte Radu. Swinir: Image restoration using swin transformer. In: *Proceedings of the IEEE/CVF international conference on computer vision 2021*:1833–1844.
28. Chen Junyu, Cai Han, Chen Junsong, et al. Deep Compression Autoencoder for Efficient High-Resolution Diffusion Models. In: *The Thirteenth International Conference on Learning Representations 2024*.
29. Crowson Katherine, Baumann Stefan Andreas, Birch Alex, Abraham Tanishq Mathew, Kaplan Daniel Z., Ship-pole Enrico. Scalable high-resolution pixel-space image synthesis with hourglass diffusion transformers. In: *Proceedings of the 41st International Conference on Machine Learning 2024*:9550–9575.
30. Perez Ethan, Strub Florian, De Vries Harm, Dumoulin Vincent, Courville Aaron. FiLM: Visual reasoning with a general conditioning layer. *32nd AAAI Conference on Artificial Intelligence, AAAI 2018*. 2018;:3942–3951.
31. Schlemper Jo, Caballero Jose, Hajnal Joseph V., Price Anthony N., Rueckert Daniel. A Deep Cascade of Con-volutional Neural Networks for Dynamic MR Image Reconstruction. *IEEE Transactions on Medical Imaging*. 2018;37(2):491–503.
32. Shanno D. F.. Conditioning of Quasi-Newton Methods for Function Minimization. *Mathematics of Computation*. 1970;24(111):647–656.
33. Amos Brandon, Kolter J. Zico. Optnet: Differentiable optimization as a layer in neural networks. In: *International conference on machine learning 2017*:136–145.
34. Zimmermann Felix F., Kolbitsch Christoph, Schuenke Patrick, Kofler Andreas. PINQI: An End-to-End Physics-Informed Approach to Learned Quantitative MRI Recon-struction. *IEEE Transactions on Computational Imag-ing*. 2024;10:628–639.
35. Zbontar Jure, Knoll Florian, Sriram Anuroop, et al. fastMRI: An open dataset and benchmarks for acceler-ated MRI. *arXiv preprint arXiv:1811.08839*. 2018;.
36. Aubert-Broche Berengère, Griffin Mark, Pike G. Bruce, Evans Alan C., Collins D. Louis. Twenty new digi-tal brain phantoms for creation of validation image data bases. *IEEE Transactions on Medical Imaging*. 2006;25(11):1410–1416.
37. Lyu Mengye, Mei Lifeng, Huang Shoujin, et al. M4Raw: A multi-contrast, multi-repetition, multi-channel MRI k-space dataset for low-field MRI research. *Scientific Data*. 2023;10(1):264.
38. El-Rewaify Hossam, Fahmy Ahmed S., Pashakhanloo Farhad, et al. Multi-domain convolutional neural network (MD-CNN) for radial reconstruction of dynamic cardiac MRI. *Magnetic Resonance in Medicine*. ;85(3):1195–1208.
39. Messroghli Daniel R., Radjenovic Aleksandra, Kozierke Sebastian, Higgins David M., Sivananthan Mohan U., Ridgway John P.. Modified Look-Locker Inversion Recov-ery (MOLLI) for High-Resolution T 1 Mapping of the Heart. *Magnetic Resonance in Medicine*. 2004;52(1):141–146.
40. Schuenke Patrick, Windschuh Johannes, Roeloffs Volkert, Ladd Mark E., Bachert Peter, Zaiss Moritz. Simultaneous Mapping of Water Shift and B1 (WASABI)-Application to Field-Inhomogeneity Correction of CEST MRI Data. *Magnetic Resonance in Medicine*. 2017;77(2):571–580.
41. Weigel Matthias. Extended phase graphs: Dephasing, RF pulses, and echoes - Pure and simple. *Journal of Magnetic Resonance Imaging*. 2015;41:266–295.
42. Hamilton Jesse I., Jiang Yun, Chen Yong, et al. MR fingerprinting for rapid quantification of myocardial T1, T2, and proton spin density. *Magnetic Resonance in Medicine*. 2017;77:1446–1458.
43. Schuenke Patrick, Redshaw Kranich Catarina, Lutz Max, et al. Open-source cardiac magnetic resonance finger-printing. *Magnetic Resonance Materials in Physics, Biol-ogy and Medicine*. 2025;.
44. Kingma Diederik P., Ba Jimmy. Adam: A Method for Stochastic Optimization. In: Bengio Yoshua, LeCun Yann, eds.. *3rd International Conference on Learning Representations, ICLR 2015, San Diego, CA, USA, May 7-9, 2015, Conference Track Proceedings 2015*.
45. Kolbitsch Christoph. *2D Cartesian MR raw data [dataset]*. Zenodo, 2025, doi: 10.5281/zenodo.15223816.
46. Zaitsev Maxim, Maclaren Julian, Herbst Michael. Motion Artifacts in MRI: A Complex Problem with Many Par-tial Solutions. *Journal of Magnetic Resonance Imaging*. 2015;42:887–901.
47. Batchelor Philip G., Atkinson David, Irarrazaval Pablo, Hill D. L. G., Hajnal Joseph, Larkman D.. Matrix Description of General Motion Correction Applied to Multishot Images. *Magnetic Resonance in Medicine*. 2005;54:1273–1280.
48. Prieto Claudia, Uribe Sergio, Razavi Reza, Atkinson David, Schaeffter Tobias. 3D Undersampled Golden-Radial Phase Encoding for DCE-MRA Using Inherently Regularized Iterative SENSE. *Magnetic Resonance in Medicine*. 2010;64:514–526.
49. Buerger Christian, Clough Rachel E., King Andrew P., Schaeffter Tobias, Prieto Claudia. Nonrigid Motion Mod-eling of the Liver From 3-D Undersampled Self-Gated Golden-Radial Phase Encoded MRI. *IEEE Transactions on Medical Imaging*. 2012;31:805–815.
50. Kolbitsch Christoph, Schattenfroh Jakob, Jaitner Noah. *Free-breathing MRI of the liver [dataset]*. Zenodo, 2025, doi: 10.5281/zenodo.15288250.
51. Block Kai Tobias, Uecker Martin, Frahm Jens. Suppres-sion of MRI Truncation Artifacts Using Total Variation Constrained Data Extrapolation.. *Int J Biomed Imaging*. 2008;2008:184123.
52. Rueckert D., Sonoda L. I., Hayes C., Hill D. L. G., Leach M. O., Hawkes D. J.. Nonrigid Registration Using Free-Form Deformations: Application to Breast MR Images. *IEEE Transactions on Medical Imaging*. 1999;18:712–721.
53. Pragliola Monica, Calatroni Luca, Lanza Alessandro, Sgallari Fiorella. On and beyond total variation regu-larization in imaging: the role of space variance. *SIAM Review*. 2023;65(3):601–685.
54. Kofler Andreas, Altekrieger Fabian, Antarou Ba Fatima, et al. Learning regularization parameter-maps for varia-tional image reconstruction using deep neural networks

- and algorithm unrolling. *SIAM Journal on Imaging Sciences*. 2023;16:2202–2246.
55. O'Reilly Thomas, Teeuwisse Wouter M., Gans Danny, Koolstra Kirsten, Webb Andrew G.. In vivo 3D brain and extremity MRI at 50 mT using a permanent magnet Halbach array. *Magnetic resonance in medicine*. 2021;85(1):495–505.
 56. Winter Lukas, Periquito Joao, Kolbitsch Christoph, et al. Open-source magnetic resonance imaging: improving access, science, and education through global collaboration. *NMR in Biomedicine*. 2024;37(7):e5052.
 57. Schote David, Silemek Berk, O'Reilly Thomas, et al. Nexus: A Versatile Console for Advanced Low-field MRI. *Magnetic Resonance in Medicine*. 2025;93(5):2224–2238.
 58. Ma Dan, Gulani Vikas, Seiberlich Nicole, et al. Magnetic resonance fingerprinting.. *Nature*. 2013;495:187–192.
 59. Captur Gabriella, Gatehouse Peter, Keenan Kathryn E., et al. A medical device-grade T1 and ECV phantom for global T1 mapping quality assurance - the T1 Mapping and ECV Standardization in cardiovascular magnetic resonance (T1MES) program. *Journal of Cardiovascular Magnetic Resonance*. 2016;18:1–20.
 60. Redshaw Kranich Catarina. *Open-Source Cardiac MR Fingerprinting [dataset]*. Zenodo, 2025, doi: 10.5281/zenodo.15726937.
 61. Wang Zhou, Bovik Alan Conrad, Sheikh Hamid Rahim, Simoncelli Eero P.. Image quality assessment: From error visibility to structural similarity. *IEEE Transactions on Image Processing*. 2004;13(4):600–612.
 62. Adler Jonas, Kohr Holger, Öktem Ozan. *Operator Discretization Library (ODL)*. 2017.
 63. Tachella Julián, Terris Matthieu, Hurault Samuel, et al. DeepInverse: A Python package for solving imaging inverse problems with deep learning. *arXiv preprint arXiv:2505.20160*. 2025;.
 64. Ong Frank, Lustig Michael. SigPy: A Python Package for High-Performance Iterative Reconstruction. In: *Proceedings of the ISMRM 27th Annual Meeting* 2019.
 65. Yiasemis George, Moriakov Nikita, Karkalousos Dimitrios, Caan Matthan, Teuwen Jonas. DIRECT: Deep Image REConstruction Toolkit. *Journal of Open Source Software*. 2022;7(73):4278.
 66. Cardoso M. Jorge, Li Wenqi, Brown Richard, et al. MONAI: An open-source framework for deep learning in healthcare. 2022;.
 67. Pinaya Walter H. L., Graham Mark S., Kerfoot Eric, et al. Generative AI for medical imaging: extending the MONAI framework. *arXiv preprint arXiv:2307.15208*. 2023;.
 68. Pérez-García Fernando, Sparks Rachel, Ourselin Sébastien. TorchIO: a Python library for efficient loading, preprocessing, augmentation and patch-based sampling of medical images in deep learning. *Computer Methods and Programs in Biomedicine*. 2021;:106236.
 69. Maier Oliver, Spann Stefan M., Bödenler Markus, Stollberger Rudolf. PyQMRI: An accelerated Python based Quantitative MRI toolbox. *Journal of Open Source Software*. 2020;5(56):2727.
 70. Karakuzu Agah, Boudreau Mathieu, Duval Tanguy, et al. qMRLab: Quantitative MRI analysis, under one umbrella. *Journal of Open Source Software*. 2020;5(53).
 71. Tamir Jonathan I., Blumenthal Moritz, Wang Jiachen, Oved Tal, Shimron Efrat, Zaiss Moritz. MRI acquisition and reconstruction cookbook: recipes for reproducibility, served with real-world flavour.. *Magnetic Resonance Materials in Physics, Biology and Medicine*. 2025;.
 72. Tatman Ben. *Quantitative Study Group: T1 [dataset]*. Zenodo, 2024, doi: 10.5281/zenodo.10868350.
 73. Tatman Ben. *Quantitative Study Group: T2* [dataset]*. Zenodo, 2024, doi: 10.5281/zenodo.10868361.
 74. Loktyushin A., Herz K., Dang N., et al. MRzero - Automated discovery of MRI sequences using supervised learning. *Magnetic Resonance in Medicine*. 2021;86:709–724.
 75. Abadi Martín, Agarwal Ashish, Barham Paul, et al. Tensorflow: Large-scale machine learning on heterogeneous distributed systems. *arXiv preprint arXiv:1603.04467*. 2016;.
 76. Uecker Martin, Lai Peng, Murphy Mark J., et al. ESPIRiT-an Eigenvalue Approach to Autocalibrating Parallel MRI: Where SENSE Meets GRAPPA.. *Magnetic Resonance Imaging*. 2013;.